Digest Journal of Nanomaterials and Biostructures Vol. 8, No. 3, July - September 2013, p. 1191 - 1203

ANTIBACTERIAL ACTIVITY OF ZINC OXIDE – GENTAMICIN HYBRID MATERIAL

G. VOICU, O. OPREA*, B. S. VASILE, E. ANDRONESCU
University Politehnica of Bucharest, Faculty of Applied Chemistry and Materials Science, Romania

Nanocrystalline ZnO particles were prepared from ethanolic solutions of zinc acetate by forced hydrolysis, at a low temperature. The fresh prepared ZnO nanoparticles were coated with gentamicin. The nanoparticles were characterized by X-ray diffraction (XRD), transmission electron microscopy (TEM) and thermal analysis (TG-DSC). The electronic (UV-Vis), infrared (FTIR) and photoluminescence (PL) spectra were also recorded. The biological activity tests such as minimum inhibitory concentration (MIC) and disk diffusion were performed in Mueller–Hinton broth using different concentrations of ZnO and ZnO-gentamicin hybrid nanoparticles, by a standard microbial method on *Enterococcus faecalis, Salmonella, Escherichia coli, Pseudomonas aeruginosa, Staphylococcus aureus and Listeria monocytogenes*. The bacteriological tests indicate a synergic activity of ZnO-gentamicin nanoparticles. The release rate of gentamicin was monitored photometrically with UV-Vis spectrometer.

(Received June 3, 2013; Accepted September 4, 2013)

Keywords: Zinc oxide, gentamicin, synergic antibacterial activity, wound dressing

1. Introduction

Zinc oxide like many semiconductors has various technical applications [1-13], but it is also used in a series of cosmetic preparates, sun protection cream, acne treatment or as a wound dressing [14-24]. Application of zinc oxide has been shown to accelerate the healing of both chronic and acute wounds and it also exhibit antibacterial and anti-inflammatory behaviour [25, 26]. ZnO effect on epithelialisation of wounds as well as its bacteriostatic property promotes it as a topical wound dressing. It can be used in treatment of various dermatitis, diaper rashes, diaper wipes, blisters, and open skin sores [27-30].

As different bacterial strains become increasingly resistant to antibiotics, the search for new strategies to deal with the diseases causing bacteria intensifies. Researchers need to identify and develop the next generation of drugs or agents to control bacterial infections [31-43].

Another major concern is related to the growth of fungal pathogens. It is difficult to control fungal growth because fungi have developed resistance to many conventional fungicides such as benzimidazoles and dicarboximides. To overcome this resistance, it is important to explore novel antifungal agents, which may replace current control strategies [44-50].

The antibacterial effect of adhesive zinc tapes on streptococci and staphylococci were described by Gilje as early as 1949 [51]. In dentistry, the antibacterial effects of zinc oxide have been reported [52]. In a study by Södeberg et al. [53], it was found that Gram-positive bacteria were the most susceptible bacterial group to zinc ion and Gram-negative aerobic bacteria were usually not inhibited. A more recent study [25] showed that nano ZnO has an enhanced bactericidal power vs. bulk ZnO against *Escherichia coli*.

*Corresponding author: ovidiu73@yahoo.com

Jones et al demonstrated the influence of the particle size, by choosing three different values: 1μm, 50-70nm and 8nm. While 8nm diameter ZnO nanoparticles showed more than 95% growth inhibition at 1mM concentration (0.008%), ZnO nanoparticles with relatively larger particle sizes (e.g. 50-70 nm) showed only 40-50% growth inhibition at 5mM [54]. The minimum inhibitory concentration (MIC) for ZnO nanoparticles with smaller size was calculated to be 1mM (0.08 mg mL^{-1}) for Staphylococcus aureus, whereas that for larger particles of ZnO was calculated to be 15mM (1.2 mg mL^{-1}).

Vlad et al. reported antifungal activity of a membrane ZnO-PU (polyurethane) at concentration of 5% and 10% ZnO up to 60 days. Such modified ZnO membranes present important antifungal properties and can be successfully used in food or biomedical applications, in order to block the formation of biofilms [55].

In this study, nanocrystalline ZnO particles were prepared through forced hydrolysis of zinc acetate under moderate conditions. The method was chosen in order to avoid contamination of ZnO nanoparticles with ions from strong bases used currently in the precipitation methods. To the best of our knowledge, this is the first study in which nano ZnO is coated with a known Gram-negative antibiotic, gentamicin, and proved to be a successful way to design a large spectrum wound dressing material. The ZnO nanoparticles were coated with gentamicin, and the hybrid material was characterised. The biological activity was tested against *Escherichia coli, Pseudomonas aeruginosa, Staphylococcus aureus, Bacillus cereus* and *Listeria monocytogenes*.

2. Experimental procedure

Zinc acetate dihydrate, $Zn(Ac)_2 \cdot 2H_2O$, with 99.9% purity was obtained from Merck. Absolute ethanol was used as received from Sigma without further purification. Gentamicin solution with a concentration of 10mg/mL was supplied by Sigma.

ZnO synthesis was done as described before [56].

ZnO-gentamicin hybrid material synthesis

The ZnO-gentamicin hybrid was obtained by a classical method for biocompatible materials. The fresh prepared ZnO (0.0813g) was suspended in 10mL gentamicin aqueous solution (10mg/mL) and ultrasonicated for 30 min and kept under stirring at 80°C for additional 24h. After centrifugation, the nanoparticles of ZnO loaded with gentamicin were taken out of the solution and dried under air at 80°C. The ZnO-gentamicin hybrid was obtained as a white-greyish powder.

3. Experimental techniques

a) Electron Microscope Images. The transmission electron images were obtained on finely powdered samples using a Tecnai^{TM} G^2 F30 S-TWIN high resolution transmission electron microscope from FEI, operated at an acceleration voltage of 300 KV obtained from a Shottky Field emitter with a TEM point resolution of 2 Å and line resolution of 1.02 Å.

b) X-ray Diffraction. X-ray powder diffraction patterns were obtained with a Shimadzu XRD6000 diffractometer, using Cu Kα (1.5406 Å) radiation operating with 30 mA and 40 kV in the 2θ range 10–70°. A scan rate of 1° min^{-1} was employed.

c) Infrared Spectroscopy. The Fourier transform infrared (FTIR) spectra were recorded using the KBr pellet technique on a Bruker Tensor 27 spectrometer in the 4000–400 cm^{-1} frequency range. A total of 30 scans and a resolution of 1 cm^{-1} were employed in getting the spectra.

d) Chemical analysis. Elemental microanalyses (carbon and hydrogen) were carried out using a Perkin-Elmer Model 2400 CHN Analyzer.

e) Thermal analysis. Thermal behaviour of the ZnO nanopowder was followed by TG-DSC with a Netzsch TG 449C STA Jupiter. Sample was placed in alumina crucible and heated with 10K·min^{-1} from room temperature to 900° C, under the flow of 20 mL min^{-1} dried air.

f) Photoluminescence spectra. Photoluminescence spectra (PL) were measured with a Perkin Elmer P55 spectrometer using a Xe lamp as a UV light source at ambient temperature, in the range 200-800 nm, with all the samples in solid state. The measurements were made with scan speed of 200 nm·min^{-1}, slit of 10 nm, and cut-off filter of 1%. An excitation wavelength of 320 nm was used.

g) Diffuse reflectance spectra measurements were made with a JASCO V560 spectrophotometer with solid sample accessory, in the domain 200-800nm, with a speed of 200nm·min^{-1}.

h) *Microbial strains*. The antimicrobial activity of ZnO and ZnO/gentamicin nanoparticles was tested onto bacterial strains recently isolated from clinical specimens as well as collection strains belonging to the following species: *Bacillus Cereus, Staphylococcus aureus ATCC 25923, Listeria monocytogenes 318* - as Gram-positive bacteria and *Pseudomonas aeruginosa ATCC 27853* and *Escherichia coli ATCC 25922* - as Gram-negative bacteria. These microorganisms are standardized for epidemiological surveillance, especially for sterility testing of medicinal products (e.g., applied by diagnostic laboratories to determine the in vitro activity of drugs) and are among the microorganisms used in public health tests. Microbial cultures were developed on solid media, Mueller-Hinton (MH) recommended for bacterial strains.

Qualitative screening. The qualitative screening was performed by an adapted diffusimetric method. After obtaining microbial suspension standardized at 0.5 McFarland from 15-18h cultures developed on solid media, culture medium plates were seeded with microbial inoculums and spotted with 5 µL from stock solution of each chemical compound. Negative (ZnO stock suspension 40 µg/mL) and positive controls (antibiotic stock solution - gentamycin 30 µg/mL) were used. The occurrence of an inhibition zone of microbial growth around the spot was interpreted as positive result.

Quantitative assay of the antimicrobial activity. MIC (Minimal Inhibitory Concentration) values for the tested compounds were determined by twofold microdilution technique, in 96 multi-well plates, starting from 300 µg/mL to 0.59 µg/mL, for each tested microbial strain. Simultaneously, there were achieved serial dilutions for DMSO in the same volume, in order to obtain the negative control. Each well was inoculated with 5µL of 0.5 Mc Farland microbial suspension. Negative (MH broth/YPG) and positive controls (MH broth/YPG and microbial inoculum) were used. The plates were incubated for 24 h at 37°C, and MICs were read as the lowest concentration of compound that inhibited the microbial growth.

i) The gentamicin release was measured photometrically by UV-spectroscopy. 2 mg of the ZnO-gentamicin hybrid sample were immersed in 10 mL aqueous phosphate buffer saline - PBS (pH=7.4) at 37^{o}C. The tubes are placed in a bench top water shaker bath at 120 rpm and 37^{o}C. The samples are drawn at predetermined time intervals after centrifugation at 12.000 rpm for 3 min. The solution is analysed for gentamicin content using UV-Vis spectrophotometer. Derivatization is done with o-phthaldialdehyde, and absorbance measurements are done at 339 nm wavelength as described in [57]. The tests were made in duplicate and the results were recorded as an average.

4. Results and discussions

The FT-IR spectra (figure 1a) recorded for the ZnO powders presents an absorption bands near 3400 cm^{-1} attributed to O-H stretching vibration, coming from the OH groups and water molecules adsorbed on nanoparticle's surface. In addition, the peak at 1634 cm^{-1} corresponds to water molecules adsorbed on the ZnO nanoparticle's surface. The two strong absorption bands were observed at 438 and 504 cm^{-1}. While the band at 438 cm^{-1} corresponds to the E1 mode of hexagonal ZnO (also Raman active) [58], the band at 504 cm^{-1} may be associated with oxygen deficiency and/or oxygen vacancy defect complex in ZnO [59]. This can be considered to prove that the ZnO powder is pure, without polymeric hydroxo-acetate species [56].

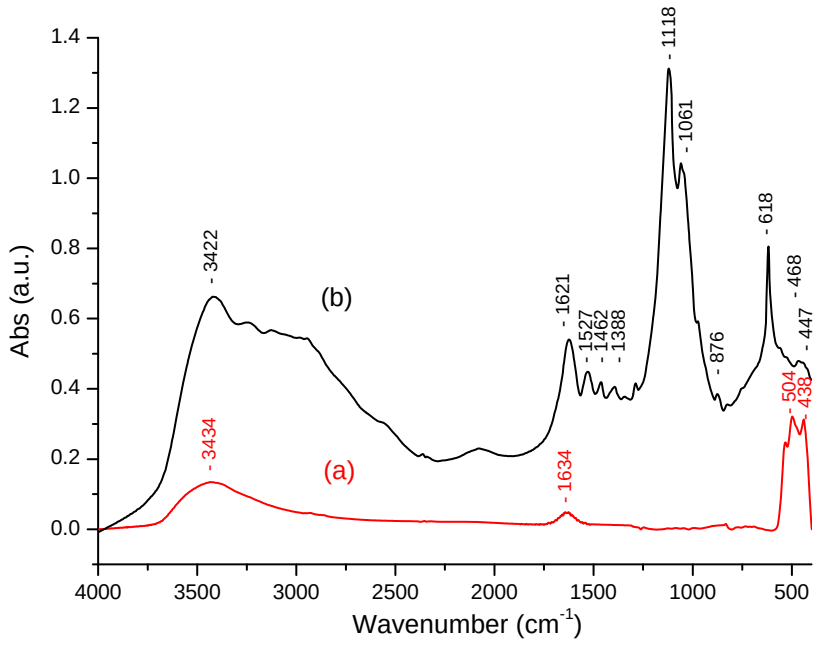

Fig. 1. The FT-IR spectra of ZnO nanopowder (a); ZnO-gentamicin nanopowder (b)

The gentamicin load of ZnO nanoparticles was also monitored by FTIR spectroscopy. Fig. 1b shows the FTIR spectra of ZnO-gentamicin nanopowder. The vibration modes of alkyl C–H stretch, amine N–H stretch and O-H stretch observed in the 2900–3420 cm^{-1} region. The NH_3^+ and NH_2^+ symmetric bend observed at 1621 and 1527 cm^{-1} are at lower energy than in free gentamicin (1637 and 1533 cm^{-1}) indicating an interaction between ZnO and these moieties [60]. The HSO_4^- stretch at 1118 cm^{-1} and SO_2 bend at 618 cm^{-1} indicates no interaction between sulphate moiety and ZnO [61]. The small intensity of the Zn-O vibration by comparison with gentamicin characteristic vibration could indicate a high load of gentamicin on the nanoparticles.

The ZnO and ZnO-gentamicin nanopowders were also investigated by **X-ray diffraction**. The XRD pattern for the ZnO nanopowder, presented in figure 2a, has proved the formation of single-phase compound, sustaining the FTIR data, demonstrating the formation of ZnO as final product. The pattern can be indexed to a hexagonal wurtzite structure. The crystallite size of the samples can be estimated from the Scherrer equation, $D = 0.89 \cdot \lambda/\beta \cdot \cos\Theta$, where D is the average grain size, λ is the X-ray wavelength (0.15405 nm), Θ and β are the diffraction angle and FWHM of an observed peak, respectively. The strongest peak (101) at $2\Theta = 36.25^o$ was used to calculate the average crystallite size (D) of ZnO particles. The estimated average crystallite size was 15,5 nm.

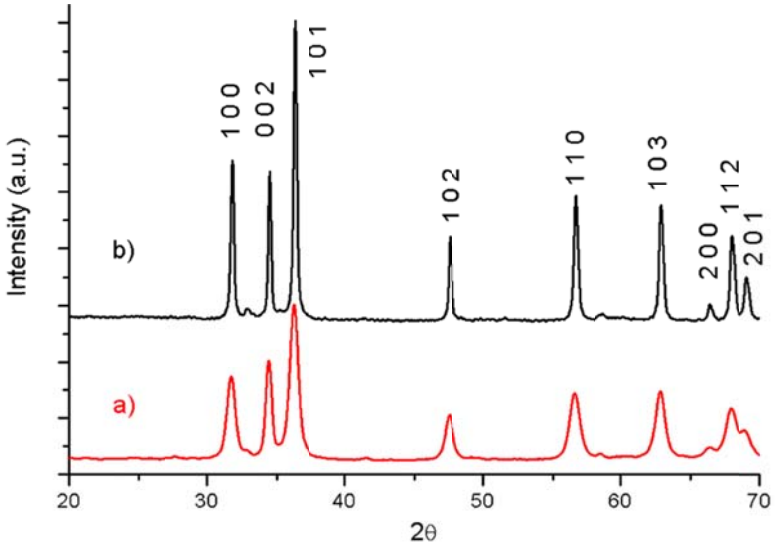

Fig. 2. XRD pattern of the ZnO nanopowder (a) ZnO-gentamicin nanopowder (b)

The XRD pattern of the ZnO-gentamicin sample, figure 2b, show that the crystalline structure of the ZnO nanoparticles is preserved after the gentamicin coating process. It is important to notice that gentamicin coating does not lead to a change in the structural or chemical properties of the nanocrystalline ZnO phase. The sharpening of the peaks is due to increase in ZnO crystallinity, as the nanopowder was allowed more time in the aqueous solution of gentamicin. No other noticeable difference can be seen between the pure ZnO and the gentamicin-loaded ZnO.

The TEM bright field image, figure 3a, obtained on uncoated ZnO reveals that the powder is composed from polyhedral shaped particles, with an average particle size of approximately 19 nm. The nanopowder presents a low tendency to form soft agglomerates.

The ZnO-gentamicin hybrid, figure 3b and 3c, shows also tendency of ZnO nanoparticles to form agglomerates. This tendency may be attributed also to the gentamicin coating that can envelop more than one particle and stick them together (figure 3c). The high-magnification images in bright field obtained for the hybrid material shows the existence of 15–20 nm individual ZnO particles, coated with a 5-6 nm film of gentamicin.

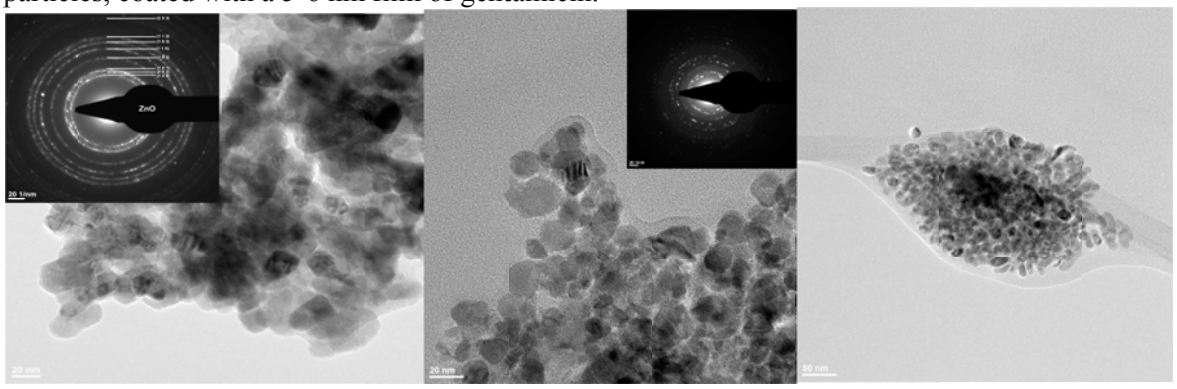

a **b** **c**

Fig. 3. TEM images of ZnO polyhedral shaped particles and SAED pattern of planes for hexagonal ZnO [ASTM 80-0075] a) uncoated; b) and c) ZnO-gentamicin nanopowder

From the selected area diffraction pattern obtained on ZnO nanopowder, uncoated and coated with gentamicin, we can state that the only phase identified is the crystalline hexagonal form of ZnO [ASTM 80-0075] for both samples. Moreover, the SAED images of both uncoated and coated ZnO confirm the Miller indices of characteristic crystalline structures identified by XRD (insets of figs. 3a and 3b).

Additional information about the structures of the nanoparticles was found through detailed analysis with HRTEM.

The HRTEM image, figure 4, shows clear lattice fringes of interplanar distances of d = 2.60 Å for nanocrystalline ZnO, corresponding to Miller indices of (0 0 2) crystallographic planes of hexagonal ZnO. In addition, the regular succession of the atomic planes indicates that the nanocrystalites are structurally uniform and crystalline with almost no amorphous phase present.

For the ZnO gentamicin hybrid material the HRTEM image indicate the lattice fringes of interplanar distances d = 2.47 Å, corresponding to Miller indices of (1 0 1) crystallographic planes of hexagonal ZnO. In addition, there is a noticeable load of amorphous phase around the nanoparticle, which was attributed to the gentamicin coating.

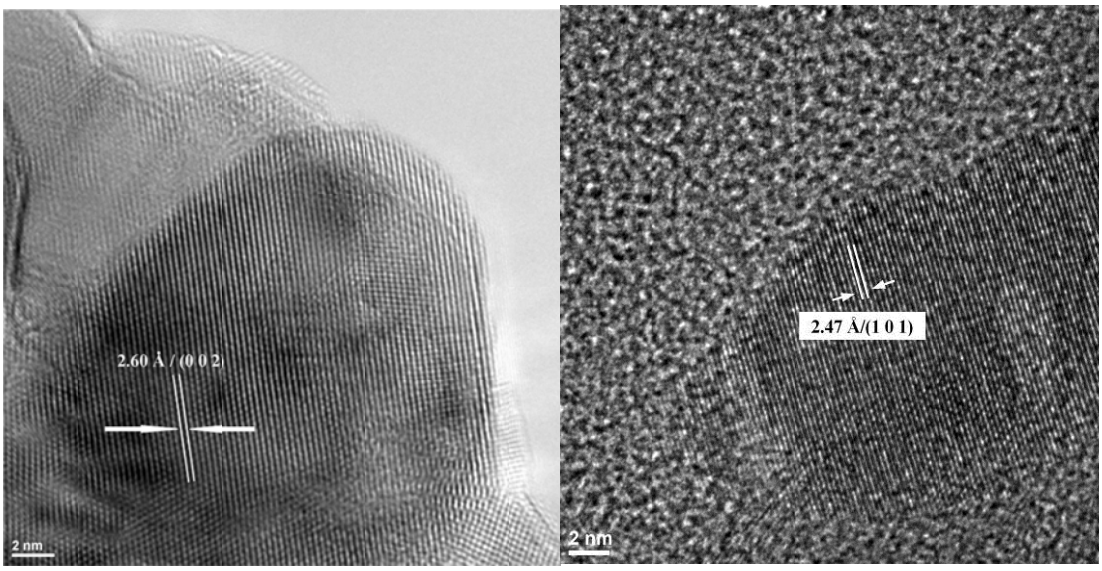

a **b**

Fig. 4. HRTEM with the crystallographic planes of ZnO nanopowder (a); ZnO-gentamicin nanopowder (b)

The photoluminescence spectrum of the as-synthesized ZnO sample presents a weak UV emission band at 394 nm, corresponding to the near band-edge emission (NBE).

The four other emission bands at 440, 456, 482, and 515 nm in the blue-green range are defect-related emissions. The high intensity of these emission bands indicates a high concentration of surface defects, as expected for polyhedral particle shape. The exact cause of them is still controversial. The luminescence bands at 440, 456 and 482 nm are believed to be caused by the transition from the level of the ionized oxygen vacancies to the valence band [62]. The 482 nm band is relatively common for semiconductor oxides like MIn_2O_4 (M = Ca, Sr, Ba) or SnO_2 [63,64] confirming that it is caused by the oxygen related defects [65,66].

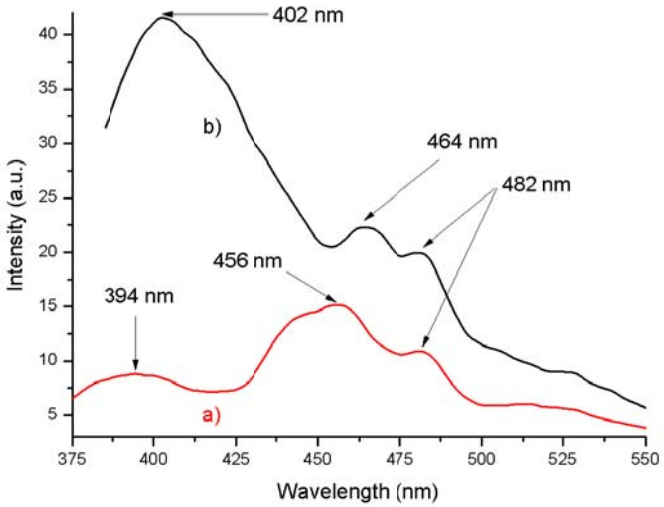

Fig. 5. Photoluminescence spectra of ZnO nanopowder (a); ZnO-gentamicin nanopowder (b)

The photoluminescence spectra of gentamicin coated ZnO presents same transitions as ZnO in the green region (482 and 515 nm) but with higher intensities. The band from 456nm in ZnO is shifted to 464nm in ZnO-gentamicin nanopowder and a new, very intense emission band appears at 402nm. The enhanced luminescence of the ZnO – gentamicin hybrid can be attributed to the presence of the organic substance and (OH) groups on the surface of the ZnO [67-69]. According to literatures, the enhancement of photoluminescence emission is caused by the removal of electron capture centres on the surface of nanocrystals or the removal of nonradiative decay channels due to the gentamicin shell [70, 71].

The electronic spectra recorded for the uncoated and gentamicin coated ZnO powder is presented in figure 6. The calculated band gap for ZnO is 3.36eV, in good agreement with the literature. The absorbance of the ZnO-gentamicin hybrid is slightly higher than that of uncoated ZnO, the layer of gentamicin contributing to the light absorption. As the spectrum is recorded in reflectance mode, the photons that are not absorbed by ZnO must travel twice through the gentamicin layer, yielding a higher absorbance. The maximum absorbance for both samples is at 362nm.

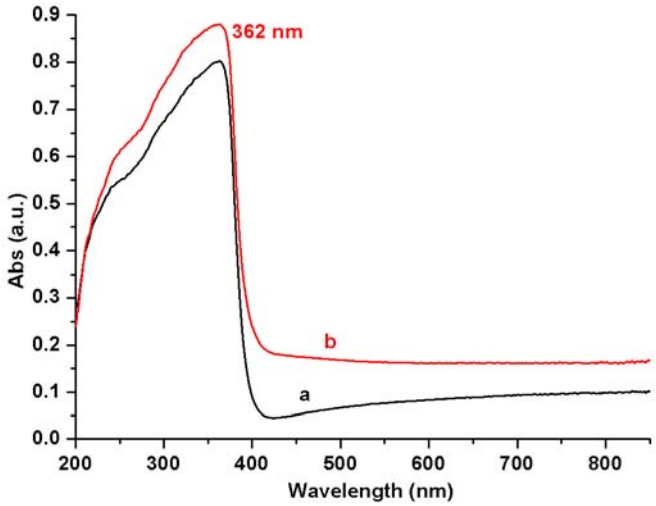

Fig. 6. Diffuse reflectance spectra of ZnO nanopowder (a); ZnO-gentamicin nanopowder (b)

The thermal analysis of ZnO-gentamicin hybrid presents three decomposition steps. First step up to 180^{o}C, with a mass loss of 5.92%, was attributed to water molecules loss. This process is accompanied by a weak endothermic effect on DSC curve.

The second decomposition step represents the beginning of the degradation of the organic molecule 220-400^{o}C, with an experimental mass loss of 16.33%. The final decomposition step takes place between 400-660^{o}C, 25.52% mass loss, and corresponds to the total combustion of the organic residue. The combustion of the organic residue is accompanied by a strong exothermic effect on DSC curve.

The residue is formed from hexagonal ZnO as indicated by XRD analysis, with a mass of representing 52.06%. The analysis is in good agreement with previously reported results for thermal behaviour of gentamicin [72].

Based on the thermal analysis results we have calculate that approximately 75% of initial quantity of gentamicin was loaded on to ZnO nanoparticles. The molar ratio of hybrid's components was calculated to be ZnO : gentamicin 6.4:1.

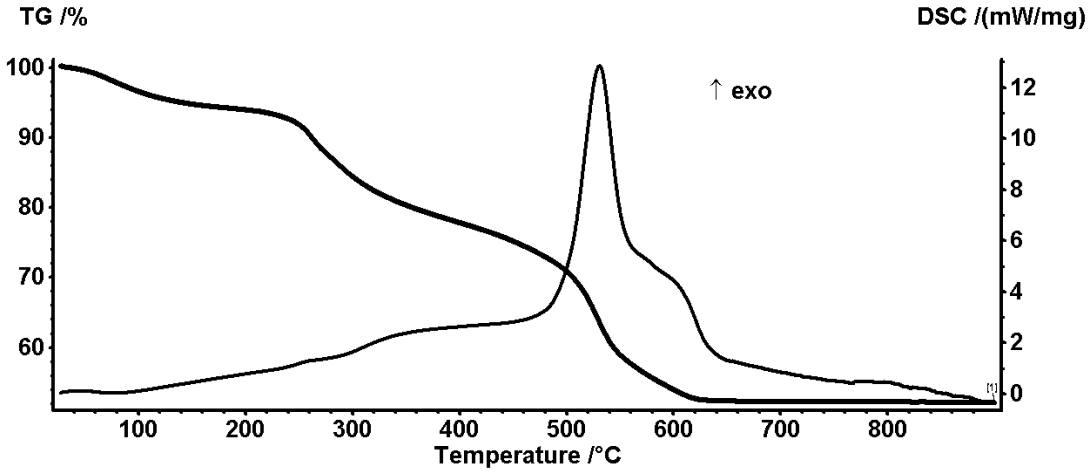

Fig. 7. Thermal analysis of ZnO-gentamicin nanopowder

Applying the disc diffusion and MIC method it was observed that the hybrid material tested has inhibitory action on the growth of five different microorganisms, *Bacillus Cereus, Escherichia coli, Pseudomonas aeruginosa, Staphylococcus aureus* and *Listeria monocytogenes*.

In the case of disc diffusion method, the experiments were conducted in comparison with standard antibiotic solution (gentamicin) by measuring inhibition zone diameters, the experimental results being shown in figure 8 and table 1. The lowest concentration (MIC, μg/mL) of the hybrid leading to an inhibitory action on the microorganisms' growth was also determined and is presented in figure 9.

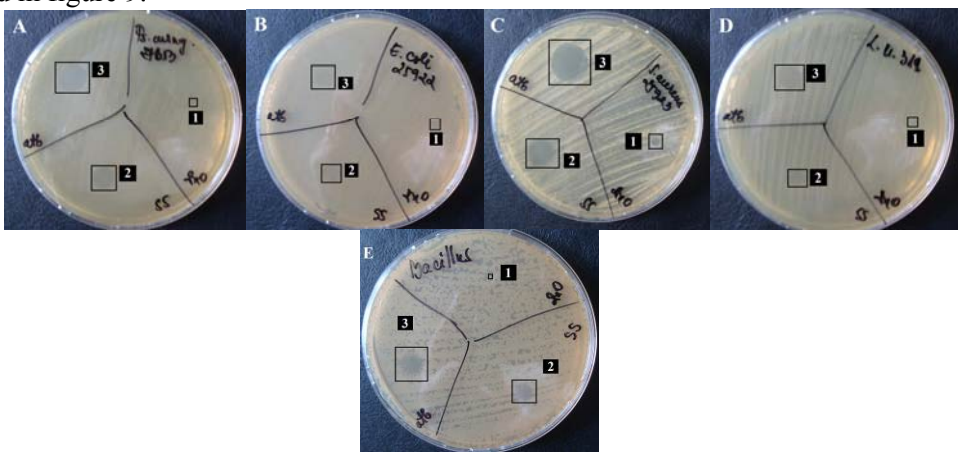

Fig. 8. Pictorial diffusion spots of A. Pseudomonas aeruginosa, B. Escherichia coli, C. Staphylococcus aureus, D. Listeria monocytogenes, E. Bacillus Cereus for 1. ZnO nanopowder, 2. Standard solution of gentamicin, 3. ZnO-gentamicin nanopowder.

Table 1. Measured inhibition zone diameters (mm) for the tested bacterial strains

Bacterial strain / Substance	Pseudomonas aeruginosa	Escherichia coli	Staphylococcus aureus	Listeria monocytogenes	Bacillus Cereus
ZnO	2	3.4	4.1	3.2	1
Gentamicin	9.5	7.6	11.8	6.7	7.6
ZnO-gentamicin	12.2	8.8	17.5	10.1	11.0

The detailed mechanism for the activity of ZnO is still under debate and is not well understood although two major hypotheses are accepted:

a) the generation of oxygen species on the surface of ZnO cause fatal damage to microorganisms; [73],

b) the binding of the particles on the bacteria surface due to the electrostatic forces followed by the cell wall rupture is the driving force behind antibacterial activity [25].

Reports in literature indicate that due to the less complex cell wall ZnO more easily inhibits the Gram-positive bacteria. From the Gram-negative strains *Escherichia coli* is particularly sensible to ZnO nanoparticles.

In present experiment, we used subinhibitory concentration of ZnO versus what is reported in [54], in order to investigate the potential influence of ZnO on gentamicin antibacterial activity. Nevertheless, the ZnO nanoparticles still presented some antibacterial activity, especially on *Staphylococcus aureus* and *Listeria monocytogenes* as Gram-positive bacteria and on *Escherichia coli* from the Gram-negative strains. We assume that the ZnO antibacterial activity even at this low concentration is due to very small particle size.

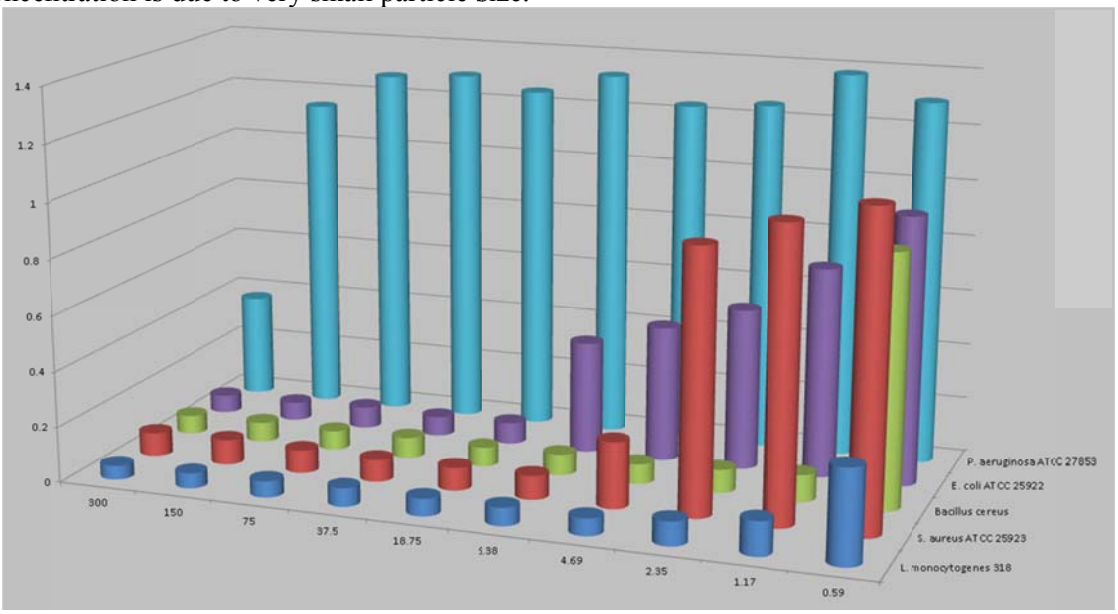

Fig. 9. MIC of ZnO-gentamicin nanopowder on the tested strains

The ZnO-gentamicin nanopowder presented an enhanced antibacterial activity on all bacterial strains when compared with the stock solution of gentamicin. The increase in inhibition zone diameters varies from 15% for *Escherichia coli* up to 51% for *Listeria monocytogenes.* High synergism activity was also exhibited on *Staphylococcus aureus* (48%) and *Bacillus Cereus* (45%) strains.

The MIC values of ZnO-gentamicin nanoparticles against the tested bacterial strains, ranged from 0.59 to 300μg/mL. *Listeria monocytogenes* was inhibited at the lowest MIC and *Pseudomonas aeruginosa* had the highest value of MIC.

The gentamicin release rate was measured to understand if the entire antibiotic amount is made available in a short period. If the gentamicin was strongly bounded on ZnO nanoparticles then the release rate should be slow.

Because the drug was adsorbed on the surface of the individual particles, the shape of the release curve presents an initial burst up to 10 min, followed by a declining release rate up to 1 hour (Figure 10).

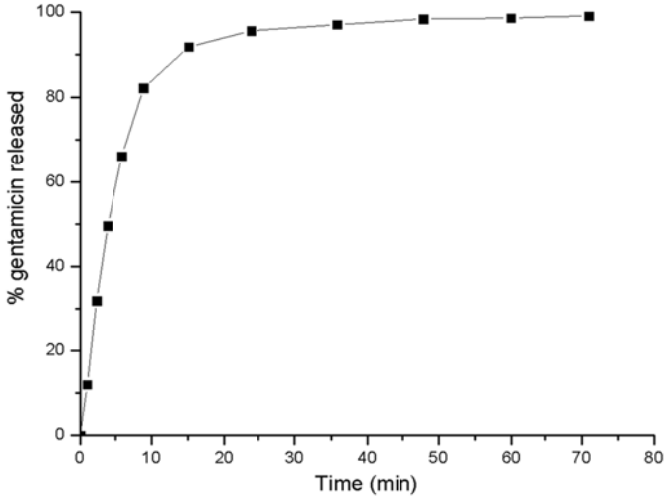

Fig. 10. The gentamicin release rate from the ZnO-gentamicin nanopowder

The fast release shows that the release kinetic is dominated by adsorption/desorption and by diffusion out of the nanoparticles clusters. This is clearly what can be expected if all the gentamicin that is loosely bound to the surface will diffuse out into the water phase, as gentamicin is highly hydrophilic. The release of gentamicin in the first hour was calculated to be ~95%.

One important parameter is the total load of drug per 1g of ZnO. The total loading can be computed as total amount of detected gentamicin. The result (0.834 g gentamicin / 1g ZnO) is in good agreement with the gentamicin content calculated from thermal analysis (47.94% gentamicin in ZnO-gentamicin nanopowder).

5. Conclusions

The ZnO particles prepared by a simple method were coated with a Gram-negative antibiotic, gentamicin. The hybrid material was characterised by FTIR, UV-Vis and fluorescence spectra, thermal analysis, TEM and XRD. The biological activity of the ZnO and ZnO-gentamicin hybrid material was tested on eight bacterial strains, good results being obtained against *Bacillus Cereus, Escherichia coli, Pseudomonas aeruginosa, Staphylococcus aureus* and *Listeria monocytogenes*. On *Enterococcus faecalis* and *Salmonella* the ZnO-gentamicin nanopowder had no inhibitory action. The results indicate a synergic activity of ZnO and gentamicin, in all cases where antibacterial activity was presented. The increase of inhibition diameters varies from 15% up to 51%, very good results being obtained for Gram-positive bacteria. In the case of *Escherichia coli* that is known to be gentamicin resistant the presence of ZnO nanoparticles is also enhancing the drug activity, but the inhibition zone is smaller.

In this study, we have demonstrated that small quantities of ZnO nanoparticles can greatly improve and increase the antibacterial activity of an antibiotic. The amount of antibiotic loaded on the ZnO nanoparticles can be adjusted by simply changing the concentration of the antibiotic solution in the synthesis step. The presented method allows loading biocompatible ZnO nanoparticles with any water/alcohol soluble drug, opening new ways in the design of wound dressing materials.

Acknowledgments

Authors recognize financial support from the European Social Fund through POSDRU/89/1.5/S/54785 project: "Postdoctoral Program for Advanced Research in the field of nanomaterials"

References

[1] C.I. Covaliu, T. Mălăeru, G. Georgescu, O. Oprea, L. Alexandrescu, I. Jitaru - Digest Journal of Nanomaterials and Biostructures, **6**(4), 1491 (2011).
[2] D. Ficai, A. Ficai, B. S. Vasile, M. Ficai, O. Oprea, C. Guran, E. Andronescu - Digest Journal of Nanomaterials and Biostructures, **6**(3), 943 (2011).
[3] C.I. Covaliu, L. C. Chioaru, L. Crăciun, O. Oprea, I. Jitaru – Optoelectron. Adv. Mater. – Rapid Comm., **5**(10), 1097 (2011).
[4] B. Johannes, S. Robin, B. Frank, A. Petia, W. Udo, B. Joachim - Biointerface research in applied chemistry, **2**(3), 339 (2012)
[5] K.S. Weißenrieder, J. Muller, Thin Solid Films. **300,** 30 (1997).
[6] F. Vaja (Dumitru), C. Comanescu, O. Oprea, D. Ficai, C. Guran - Revista de Chimie – **63**(7), 722 (2012).
[7] J. Neamtu, C.M. Teodorescu, G. Georgescu, J. Ferre, T. Malaeru, I. Jitaru, *Structural and Magneto-Optical Properties of Co-doped ZnO Thin Films Prepared by Sol-Gel Method,* NSTI NANOTECH 2008.,TECHNICAL, vol.1, 2008, pp. 238-241, ISBN**:** 978-1-4200-8503-7
[8] A. Radu, S. Iftimie, V. Ghenescu, C. Besleaga, V.A. Antohe, G. Bratina, L. Ion, S. Craciun, M. Girtan, S. Antohe, Dig J Nanomater Bios. **6**, 1141 (2011).
[9] S. Ghosh, V. Sih, W. H. Lau, D. D. Awschalam, S.-Y. Bae, S. Wang, S.Vaidya, G. Chapline, Appl. Phys. Lett. **86**, 232507 (2005).
[10] F. Vaja (Dumitru), D. Ficai, A. Ficai, O. Oprea, C. Guran – J. Optoelectron. Adv. Mater. **15**(1- 2), 107 (2013).
[11] O. Oprea, O. R. Vasile, G. Voicu, L. Craciun, E. Andronescu - Dig J Nanomater Bios. – **7**(4), 1757 (2012).
[12] O.R. Vasile, E. Andronescu, C. Ghitulica, B.S. Vasile, O. Oprea, E. Vasile, R. Trusca – Journal of Nanoparticle Research, (2012) 14:1269, DOI: 10.1007/s11051-012-1269-7
[13] G. Voicu, O. Oprea, B.S. Vasile, E. Andronescu - Dig J Nanomater Bios. **8**(2), 667 (2013).
[14] D.H. Yan, G. Yin, Z. Huang, M. Yang, X. Liao, Y. Kang, Y. Yao, B. Hao, D. Han - Journal of Physical Chemistry B, **113**(17), 6047 (2009).
[15] S. Gonzalez, Y. Gilaberte, N. Philips, A. Juarranz - The Open Dermatology Journal, **5**, 6 (2011).
[16] B.Y. Reddy, B.M. Hantash - The Open Dermatology Journal, **3**, 22 (2009).
[17] G. Gambarini, L. Testarelli, D. Al-Sudani, G. Plotino, N. Grande, A. Lupi, B. Giardina, G. Nocca, M. Luca - The Open Dentistry Journal, **5**, 29 (2011), p.
[18] C.G. Burkhart, C. Black, C.N. Burkhart - The Open Dermatology Journal, **3**, 11 (2009).
[19] V.E. Copcia, R. Gradinaru, G.D. Mihai, N. Bilba, I. Sandu - Revista de Chimie, **63**(11), 1124 (2012).
[20] J. Baier, R. Strumberger, F. Berger, P. Atanasova, U. Welzel, J. Bill - Biointerface research in applied chemistry, **2(**3), 339 (2012).
[21] J. Baier, T. Naumburg, N. Blumenstein, L. Jeurgens, U. Wezel, T. Do - Biointerface research in applied chemistry, **2**(4), 380 (2012).
[22] J. Hai-Bo, F.N. Oktar, S. Dorozhkin, S. Agathopoulos - Journal of Composite Materials, **45**(13), 1435 (2010)
[23] O. Gunduz, E. Erkan, S. Daglilar. S. Salman, S. Agathopoulos, F.N. Oktar - Journal of Material Science, **43**(8), 2536 (2008).
[24] L.S. Ozyegin, F.N. Oktar, N. Heybeli - Key Engineering Materials, **240-242**, 349 (2003).
[25] N. Padmavathy, R. Vijayaraghavan - Sci. Technol. Adv. Mater. **9**, 035004 (2008)
[26] S. Atmaca, K. Gul, R. Cicek - Tr. J. of Medical Sciences, **28**, 595 (1998), p.
[27] K.T. Shalumon, K.H. Anulekha, S.V. Nair, S.V. Nair, K.P. Chennazhi, R. Jayakumar- International Journal of Biological Macromolecules, **49**(3), 247 (2011) p.
[28] P.T.S. Kumar, V.K. Lakshmanan, T.V. Anilkumar, C. Ramya, P. Reshmi, A.G. Unnikrishnan, S.V. Nair, R. Jayakumar- Acs Applied Materials & Interfaces, **4(**5), 2618 (2012).
[29] S.K. Rajashri, B. Amruta, P.B. Vrinda, S.R. Koyar - Biointerface research in applied

chemistry, **1**(2), 57 (2011).
[30] R.S. Subhasree, D. Selvakumar, N.S. Kumar - Letters in Applied NanoBioScience, **1**(1), 2 (2012).
[31] A.M. Grumezescu, E. Andronescu, A. Ficai, D.E. Mihaiescu, B.S. Vasile, C. Bleotu - Letters in Applied NanoBioScience, **1**(2), 31 (2012).
[32] S. Selvam, R. Rajiv Gandhi, J. Suresh, S. Gowri, S. Ravikumar, M. Sundrarajan – International Journal of Pharmaceutics, **434**(1-2), 366 (2012).
[33] R. Olar, M. Badea, M. Ilis, Ticuţa Negreanu-Pîrjol, M. Călinescu - Journal of Thermal Analysis and Calorimetry, **111**(2), 1189 (2013), p.
[34] E. Andronescu E, A.M. Grumezescu, A. Ficai, I. Gheorghe I, M. Chifiriuc, D.E. Mihaiescu – Biointerface research in applied chemistry, **2**(3), 332 (2012).
[35] S.P. Chakraborty, S.K. Sahu, P. Pramanik, S. Roy - International Journal of Pharmaceutics, **436**(1-2), 659 (2012).
[36] A.M. Grumezescu, E. Andronescu, A. Ficai, C. Bleotu, M.C. Chifiriuc - Biointerface research in applied chemistry, **2**(5), 438 (2012).
[37] J. Gautier, E. Munnier, A. Paillard, K. Herve, L. Douziech-Eyrolles, M. Souce - International Journal of Pharmaceutics, **423**(116), (2012).
[38] T. Negreanu-Pîrjol, M. Bratu, M. Arcuş, M. Giurginca, C. Guran - Revista de Chimie, **57**(6), 575 (2006).
[39] A.M. Grumezescu, A.M. Holban, E. Andronescu, A. Ficai, C. Bleotu, M.C. Chifiriuc - Letters in Applied NanoBioScience, **1**(4), 77 (2012).
[40] C. Saviuc, A.M. Grumezescu, A. Holban, C. Bleotu, C. Chifiriuc, P. Balaure - Biointerface research in applied chemistry, **1**(3), 111 (2011).
[41] Y. Li, X. Zheng, Z. Cao, W. Xu, J. Zhang, M. Gong - International Journal of Pharmaceutics, **434**(1-2), 209 (2012),
[42] L. Bucur, T. Negreanu-Pîrjol, M. Giurginca, V. Istudor - Revue Roumaine de Chimie, **53**(10), 961 (2008), p.
[43] A.M. Grumezescu, E. Andronescu, A. Ficai, D. Ficai, K.S. Huang, I. Gheorghe - Biointerface research in applied chemistry, **2**(6), 469 (2012), p.
[44] D.E. Mihaiescu, M. Horja, I. Gheorghe, A. Ficai, A.M. Grumezescu, C. Bleotu - Letters in Applied NanoBioScience, **1**(2), 45 (2012).
[45] T. Negreanu-Pîrjol, B. Negreanu-Pîrjol, R. Sîrbu, G. Paraschiv, A. Meghea - Journal of Environmental Protection and Ecology, **13**(3A), 1744 (2012).
[46] C. Saviuc, A.M. Grumezescu, A. Holban, C. Chifiriuc, D. Mihaiescu, V. Lazar - Biointerface research in applied chemistry, **1**(2), 64 (2011).
[47] L. Jia, J. Shen, Z. Li, D. Zhang, Q. Zhang, C. Duan - International Journal of Pharmaceutics, **439**(1-2), 81 (2012).
[48] D.E. Mihaiescu, A.M. Grumezescu, P.C. Balaure, D.E. Mogosanu, V. Traistaru - Biointerface research in applied chemistry, **1**(5), 191 (2011).
[49] R. Sîrbu, C. Ursache, T. Zaharia, S. Nicolaev, T. Negreanu-Pîrjol, B. Negreanu-Pîrjol, R.M. Stoicescu - Journal of Environmental Protection and Ecology, **13**(3A), 1865 (2012), p.
[50] A.M. Grumezescu, E. Andronescu, A. Ficai, C. Bleotu, D.E. Mihaiescu, M.C. Chifiriuc – International Journal of Pharmaceutics, **436**(1-2771), (2012), p.
[51] O.H. Paetzold, A. Wiese - Arch. Derm. Res. **253**, 151 (1975),
[52] W.R. Moore, J.M. Genet - Oral Surgery **53**, 508 (1982),
[53] T.A. Södeberg, B. Sunze, S. Holm, T. Elmro, G. Hallmans, S. Sjöberg - Scand. J. Plast. Reconstr. Hand. Surg. **24**, 193 (1990).
[54] N. Jones, B. Ray, KT Ranjit, AC Manna - FEMS Microbiology Letters, **279**(1), 71 (2008).
[55] S. Vlad, C. Tanase, D. Macocinschi, C. Ciobanu, T. Balaes, D. Filip, I.N. Gostin, L.M. Gradinaru - Dig J Nanomater Bios., **7**(1), 51 (2012).
[56] O. Oprea, E. Andronescu, B.S. Vasile, G. Voicu, C. Covaliu - Dig J Nanomater Bios. **6**(3), 1393 (2011), p.
[57] D.H. Robinson, S.S. Sampath - J. Pharm. Sci. **79**(5), 428 (1991).
[58] G. Xiong, U. Pal, J.G. Serrano, K.B. Ucer, R.T. Williams - Phys. Stat. Sol. (C) **3**(10), 3577 (2006).

[59] A. Kaschner, U. Haboeck, M. Strassburg, G. Kaczmarczyk, A. Hoffmann, C. Thomsen, A. Zeuner, H.R. Alves, D.M. Hofmann, B.K. Meyer - Appl. Phys. Lett. **80**, 1909 (2002).
[60] H. Pandey, V. Parashar, R. Parashar, R. Prakash, P.W. Ramteke, A.C. Pandey - Nanoscale, **3**(10), 4104 (2011).
[61] N. Manjunatha, S. Vasanti, N. Rajesh, N. Uma - Int.J. PharmTech. Res. **2**(1), 856 (2010).
[62] O. Oprea, O.R. Vasile, G. Voicu, E. Andronescu - Dig J Nanomater Bios. **8**(2), 747 (2013), p.
[63] D. Gingasu, O. Oprea, I. Mindru, D. C. Culita, L. Patron, Dig J Nanomater Bios. **6,** 1215 (2011).
[64] A.M. Ungureanu, I. Jitaru - Bull Sci UPB, B Series, **76**(3), (2013)
[65] Y. Zhu, Y. Chen, X. Zhang - European Journal of Chemistry **2**, 8 (2011), p
[66] N.S. Sabri, A..K. Yahya, M.K. Talari - Journal of Luminescence **132**, 1735 (2012).
[67] H. Zhou, H. Alves, D. M. Hofmann, B. K. Meyer, G. Kaczmarczyk, A. Hoffmann, C. Thomsen - Phys. Stat. Sol. (B) **229**(2), 825 (2002), p
[68] D. Jiang, L. Cao, G. Su, H. Qu, D. Sun - Applied Surface Science **253**, 9330 (2007).
[69] L Peng, Y Wang - Nanoscale Res Lett **5**, 839 (2010).
[70] Y. Zhang, Y.D. Li, J. Phys. Chem. B, **108**, 17805 (2004),
[71] Q. Liu, W. Ren, Y. Zhang, Y.X. Zhang - European Polymer Journal **47**, 1135 (2011).
[72] W. Simchua, N.A. Narkkong, Y. Baimark - Research Journal of Nanoscience and Nanotechnology, **1**, 34 (2011), p.
[73] K. Sunada, Y. Kikuchi, K. Hashimoto, A. Fujshima - Environ. Sci. Technol. **32**, 726 (1998).